Range Image Registration Using Hierarchical Segmentation and Clustering

Yonghuai Liu
Department of Computer Science
Aberystwyth University
Ceredigion SY23 3DB, UK

Longzhuang Li
Department of Computing Sciences
Texas A and M University
Corpus Christi, TX 78412, USA

Xianghua Xie
Department of Computer Science
Swansea University
Swansea SA2 8PP, UK

Baogang Wei
College of Computer Sciences
Zhejiang University
Hangzhou 310027, P.R. China

***Abstract*— An accurate, robust, and automatic registration of overlapping range images is usually a pre-requisite step for range image analysis and applications. While accurate depiction of object geometry requires the increase of the resolutions of images and thus, the amount of data to process, an efficient processing of such data then usually becomes an issue. In this paper, we first employ the efficient tensor analysis and k means clustering methods to hierarchically segment and cluster the original range images into a small number of planar patches represented as the closest points in the original images to their centroids. Then an advanced ICP variant is adopted to register such closest points. Finally, another ICP variant is used to refine the registration results obtained over all the points in the images. The experimental results based on real range images show that the proposed technique significantly outperforms the selected two state of the art ones for accurate and efficient registration of overlapping range images.**

I. Introduction

The latest laser scanning technologies enable the acquisition of both depth and intensity information about the objects of interest in the form of range and/or intensity images (Figure 1). Since the laser scanning systems (range cameras) have a limited field of view, a number of images have to be captured from different viewpoints so that a full coverage of the object surface can be obtained. All these images are depicted in local laser scanning system centred coordinate frames. To construct a full model of the object and/or fuse the geometrical and optical information in these images, all these images usually have to be aligned into a single global coordinate frame. This process is called registration. Range image registration has two goals: one is to establish correspondences between overlapping range images, the other is to estimate the camera motion parameters that bring one range image into the best possible alignment with the other. Fixing either of these two goals renders the other trivial. However, they are in practice interwoven, complicating the range image registration process.

A. Previous work

Range image registration is a fundamental problem in numerous applications of the latest laser scanning technologies such as 3D object modelling and recognition. As a result, a large number of automatic algorithms have been developed in the literature. These algorithms can be classified into three main categories with regard to the order between the establishment of possible correspondence and the evaluation of camera motion parameters: (1) feature extraction and matching [5], [4]; (2) an optimal combination of points [3], [2], and (3) camera motion search and its evaluation [10], [13]. Different categories classified here are not exclusive from each other. They can be either alternative or complementary [10], [12]. Each category has its own advantages and disadvantages:

- The first class of algorithms can establish correspondences between any two overlapping range images subject to either small or large camera motions, while the second and third classes of algorithms require that the camera motion be either approximately known or small;
- The first class of algorithms has to extract and match geometrical and/or optical features from range images, while the second and third classes of algorithms do not need to extract and match any feature at all;
- While the extraction of features is often sensitive to noise caused by point sampling on the object surface, surface orientations, reflectance properties, and the electronic and mechanical errors, the matching of the extracted features is usually not straightforward due to the fact that: (1) the similarity metric must be powerful in distinguishing between different features; and (2) since the features attached to a point in one image have to match those attached to each candidate in another, the established point matches could be entirely wrong. The second class of algorithms heavily depends on both optimization and explicit outlier modelling. In contrast, while the third class of algorithms has an advantage of finding the global optimal solution, it is usually time consuming and difficult to determine the termination conditions; and
- The second class method [10], [12] is usually employed to refine the registration results of the first and third

class methods and thus, plays a more fundamental role for accurate and efficient registration of overlapping range images.

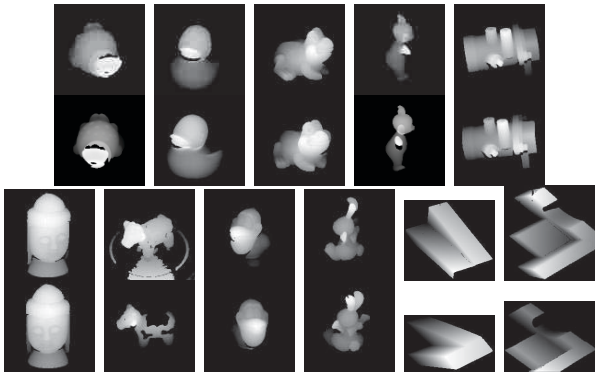

Fig. 1. Real range images used. From left column to right column and first to second in every two rows: lobster80 and 60, duck80 and 60, frog100 and 80, tubby100 and 80, valve10 and 0, buddha20 and 0, cow42 and 39, bird20 and 60, bunny100 and 60, block1-1 and 2, and curvblock1 and 2.

Consequently, automatic range image registration still remains open and advanced algorithms need to be developed.

B. Our work

Currently, the manufacturing of laser scanners has a tendency to increase their resolutions and fields of view so that the accuracy for the representation of the geometry of the object of interest can be increased. The increase of either resolution or field of view implies that the data captured increases usually quadratically. For example, while a Minolta Vivid 700 range scanner has a resolution of 200×200 and a field of view of about 40° and capture 40,000 points in a single range image, a Leica HDS6000 scanner has a resolution of as high as 1024×1024 and a field of view of as large as 360° and capture as many as 1 million points. The latter has 25 times as many points as the former. In this case, computationally efficient approaches to process such a huge amount of data are desperately needed to be developed.

The most effective way to efficiently process such range images may be to reduce the number of points. If so, then the remaining problem is how to select a subset of points from the original range images. Various techniques have been proposed in the literature such as uniform resampling [7], random sampling [5], normal space sampling [12], and multi-resolution [6]. These methods have a common shortcoming that their performance is usually unstable due to uncertainty in sampling and poor initialization and representation of the geometry in the range images.

While the existing segmentation methods [1] mainly concern the composition of range images and thus, are usually computationally intensive, we in this paper propose to use the efficient tensor analysis and k means clustering methods to hierarchically segment and cluster the original images into a small number of planar patches. Each patch is represented as the closest point in the original image to its centroid. Since ICP variants are guaranteed to establish high quality possible correspondences [9], an advanced ICP variant (EvolICP) [8] is then adopted to register these closest points. Due to the complexity of hierarchical segmentation and clustering, the registration results obtained are normally not very accurate and need to be further refined. As such, the efficient ICP variant-iterative closest reciprocal point (ICRP) [11] is finally employed to refine the registration results obtained using all the points in the original images.

To validate the performance of the proposed hierarchical segmentation and clustering (HSC) algorithm for efficient and accurate range image registration, the normal space sampling (NSS) method [12] and the spin image extraction and matching (SI) method [5], [4] were selected. All selected algorithms have an advantage of easy implementation. The NSS method samples the same number of points in the normal space as that of the planar patches in the proposed HSC algorithm and they then use the same procedures to roughly align the given images and finally refine the registration results obtained. The SI method extracts and matches spin images from range images for possible correspondences, resulting in the given images being roughly aligned. For a fair comparison, its results are also refined using the same ICRP algorithm as either the proposed HSC or NSS method does. Such comparative study is valuable, since the comparison can reveal which method provides more reliable and accurate initial registration results for the ICRP algorithm to refine: EvolICP based on hierarchical segmentation and clustering generated points or randomly sampled points in the normal space; or the feature extraction and matching method. It appears that the efficient variant of the ICP algorithm as proposed in [12] is a better candidate for comparison. However, we experimentally found that it is too sensitive to initial registration parameters to be selected for comparison. The comparative study is based on real range images (Figure 1) downloaded from a publicly accessible range image database currently hosted by the Signal Analysis and Machine Perception Laboratory at Ohio State University. While the block range images were captured using the MSU Technical Arts 100X range scanner with varied resolutions from 119×193 to 225×216 and include objects with planar surfaces, all others were captured using a Minolta Vivid 700 range camera with a fixed resolution of 200×200 pixels and include objects with free form surfaces respectively.

The rest of this paper is structured as follows: while Section II describes the novel HSC algorithm, Section III presents the experimental results. Finally, Section IV draws some conclusions.

II. Hierarchical segmentation and clustering based registration

In this section, we describe the novel HSC algorithm for efficient and accurate registration of two given overlapping range images, which are represented as point clouds: $\mathbf{P}$=$\{\mathbf{p}_1, \mathbf{p}_2, \cdots, \mathbf{p}_{n_1}\}$ and $\mathbf{P}'$=$\{\mathbf{p}'_1, \mathbf{p}'_2, \cdots, \mathbf{p}'_{n_2}\}$. Due to occlusion, appearance and disappearance of points in either cloud, n_1 is not necessarily equal to n_2. The points with the same

Fig. 2. The registration results of the proposed HSC algorithm applied to different images with the number α of patches represented as a percentage of the number of total points in the original image taking different values. Top three: lobster80-60; Bottom three: duck80-60. Left column: $\alpha = 0.5\%$; Middle column: $\alpha = 1\%$; Right column: $\alpha = 10\%$.

subscript do not mean that they are correspondences. The following notations are used throughout this paper: capital letters denote vectors or matrices, lower case letters denote scalars, $\mathbf{a} \cdot \mathbf{b}$ denotes the dot product between two vectors $\mathbf{a}$ and $\mathbf{b}$, and superscript T denotes the transpose of a vector or a matrix.

Fig. 3. The registration results of the proposed HSC algorithm applied to different images with each patch represented using different methods. Left two: frog100-80; Right two: tubby100-80. Odd columns: centroids; Even columns: closest points.

A. Tensor analysis

Given a set of points $\mathbf{p}_i$ in 3D space, the tensor analysis can be applied. The centroid $\bar{\mathbf{p}}$ of these points $\mathbf{p}_i$ can be computed as: $\bar{\mathbf{p}} = \frac{1}{n_1}\sum_{i=1}^{n_1}\mathbf{p}_i$ and their covariance matrix $\mathbf{A}$ can be computed as: $\mathbf{A}=\sum_{i=1}^{n_1}(\mathbf{p}_i - \bar{\mathbf{p}})(\mathbf{p}_i - \bar{\mathbf{p}})^T$.

Let the singular value decomposition of the 3×3 covariance matrix $\mathbf{A}$ be: $\mathbf{A} = \mathbf{U}\mathbf{W}\mathbf{U}^T = (\mathbf{e}_{max} \quad \mathbf{e}_{mid} \quad \mathbf{e}_{min}) \begin{pmatrix} \lambda_{max} & 0 & 0 \\ 0 & \lambda_{mid} & 0 \\ 0 & 0 & \lambda_{min} \end{pmatrix} \begin{pmatrix} \mathbf{e}_{max}^T \\ \mathbf{e}_{mid}^T \\ \mathbf{e}_{min}^T \end{pmatrix}$ where the diagonal elements of $\mathbf{W}$ are the eigenvalues λ_{max}, λ_{mid} and λ_{min} of $\mathbf{A}$ and the columns of $\mathbf{U}$ are the corresponding normalized eigenvectors $\vec{e}_{max}$, $\vec{e}_{mid}$ and $\vec{e}_{min}$. Since $\mathbf{A}$ is symmetric positive semi-definite, its eigenvalues λ_{max}, λ_{mid} and λ_{min} are all non-negative. These mutually perpendicular eigenvectors define the three axis directions of a local coordinate frame with origin at $\bar{\mathbf{p}}$. The eigenvalue λ_{min} measures the deviation of a set of points from a plane that passes through $\bar{\mathbf{p}}$ and is spanned by the two eigenvectors $\vec{e}_{max}$ and $\vec{e}_{mid}$ corresponding to the two largest eigenvalues λ_{max} and λ_{mid}. So $Err = \lambda_{min}/(\lambda_{max} + \lambda_{mid} + \lambda_{min})$ is defined in this paper to measure the extent to which a set of points is coplanar. The smaller the error Err, the more likely the set of points is coplanar. It is used in this paper as an indicator whether a set of points needs to be split.

B. Hierarchical segmentation and clustering

Each cluster C_k is represented by four parameters: the centroid $\mathbf{cen}_k$, the index array $\mathbf{Ind}_k$, the main axis $\mathbf{e}_k$, and Err_k. $\mathbf{cen}_k$ is the centroid of the cluster k. The array $\mathbf{Ind}_k$ records the subscripts of all the points in the cluster: $\mathbf{Ind}_k = \{k_1, k_2, \cdots, k_{n_k}\}$. $\mathbf{e}_k$ records the main axis $\mathbf{e}_{k,max}$ of the local coordinate system through the tensor analysis in the last section.

At the beginning of segmentation, the error Err is usually larger than a threshold ρ (0.001 in this paper) and the number of points in the cluster is larger than 4. Then we select the cluster C_m with the largest error Err and split this cluster into two smaller clusters. To this end, the k means clustering method is applied (k=2 in this case). To initialize the k means clustering, (1) all the points in the cluster C_m that lie on the left and right hand sides with respect to $\mathbf{e}_m$ from $\mathbf{cen}_m$ are selected: if $(\mathbf{p}_{m_j} - \mathbf{cen}_m) \cdot \mathbf{e}_m > 0$, then point $\mathbf{p}_{m_j}$ lies on the right hand side. Otherwise, it lies on the left hand side; (2) the centroids $\mathbf{cen}_{m,1}$ and $\mathbf{cen}_{m,2}$ of the points on the two hand sides are calculated respectively. Then the k means clustering method is applied to split the cluster C_m into two smaller clusters. When either the members in each cluster do not change or the maximum number (10 in this paper) of iterations has been reached, it terminates.

To save space, we always use one of the two new clusters to replace the original one C_m. In this case, after each split, the overall number of clusters is increased by one, rather than two.

C. Outline of the HSC algorithm

The proposed hierarchical segmentation and clustering based registration algorithm is summarised as follows:

1) Initialize the cluster representation using all the points in each range image
2) Initialize the maximum numbers M_1 and M_2 of patches to be segmented in the two images being registered
3) Use the pure translational motion derived from the centroid difference between the two overlapping range images being registered to initialize the registration parameters
4) For images $\mathbf{P}$ and $\mathbf{P}'$, use the approaches described in the previous two sections to do the iterative hierarchical segmentation and clustering respectively until either the maximum number of patches has been reached or the selected cluster cannot be further split, yielding centroids $\mathbf{cen}_i (i = 1, 2, \cdots, N_1)$ and $\mathbf{cen}'_j (j = 1, 2, \cdots, N_2)$, respectively.

5) Find the closest points $\mathbf{q}_i$ and $\mathbf{q}'_j$ in $\mathbf{P}$ and $\mathbf{P}'$ to $\mathbf{cen}_i$ and $\mathbf{cen}'_j$ respectively
6) Use the method in [8] to register points $\mathbf{q}_i$ and $\mathbf{q}'_j$
7) Use the ICRP algorithm in [11] to refine the registration results obtained over $\mathbf{P}$ and $\mathbf{P}'$

In the experiments described below, the following values were used: $M_1 = 0.1n_1$ and $M_2 = 0.1n_2$.

III. Experimental results

In this section, we report the experimental results for the validation of performance of the proposed HSC algorithm for accurate and efficient registration of overlapping range images. The experimental results are presented in Figures 2 through 5 and Tables I through IV. RC denotes reciprocal correspondence [11], [8]. The rotation angle of the camera motion around an unknown axis for the images captured using the Minolta Vivid 700 range camera can be derived from the image file name and thus, is one parameter of interest. In the figures, yellow colour represents the transformed images $\mathbf{P}$, the green colour represents the reference images $\mathbf{P}'$.

A. The number of planar patches

The numbers M_1 and M_2 of planar patches play a key role for the representation of the original range images and are determined by the geometries that the range images include. Too small a number of patches can hardly retain the information in the original range images and thus adversely affect the registration results. Too large a number of patches will not help reduce the computational cost of the range image registration. In this section, we experimentally investigate the effect of the number α of patches to be segmented on the final registration results. The number α of patches is represented as a percentage of the total points in the original image and is varied from 0.5%, 1%, to 10%. Two pairs of overlapping images, lobster80-60 and tubby80-60, as illustrated in Figure 1, were selected for the experiments. The experimental results are presented in Figure 2 and Table I.

Figure 2 and Table I show that when $\alpha = 0.5\%$, the proposed HSC method failed to register the lobster80-60 images. When $\alpha = 1\%$, it inaccurately registered the duck80-60 images, increasing the average registration error by as much as 16.67%. The inaccurate registration results have been manifested as the fact that the two lobster images intersect in 3D space and the beaks of the duck in the two duck images are clearly separate. Thus, in the rest of this paper, we let $\alpha = 10\%$.

B. Patch representation

In this section, we investigate how to represent the segmented patches so that more accurate registration results can be obtained. To this end, two pairs of overlapping images, frog100-80 and tubby100-80, as illustrated in Figure 1, were used for the experiments. The experimental results are presented in Figure 3 and Table II.

Figure 3 and Table II show that the representation of segmented patches using the closest points in the original range images yields slightly more accurate registration results than using the centroids especially in the sense of the estimated rotation angle of the camera motion. For example, while the former produced an error of 0.45% in the estimation of the rotation angle of the camera motion for the registration of the tubby100-80 images, the latter produced an error of 3.08%. Thus, in the rest of this paper, we will always use the closest points for the representation of the segmented patches.

C. Performance refinement

In this section, we use experiments to show that it is usually necessary to use the ICRP algorithm to refine the registration results obtained by the initial HSC algorithm, due to the complexity of hierarchical segmentation and clustering. The block1-1-2 and curvblock1-2 images (Figure 1) were used for the experiments. The experimental results are presented in Figure 4 and Table III.

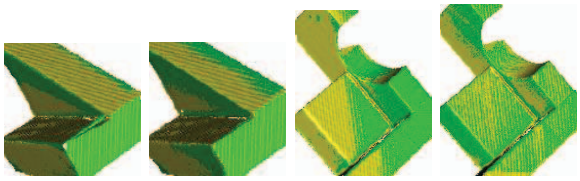

Fig. 4. The registration results of the proposed HSC algorithm applied to different images with and without refinement. Left two: block1-1-2; Right two: curvblock1-2. Odd columns: No; Even columns: Yes.

From Figure 4 and Table III, it can be seen that even though the partial HSC method produced good results in the sense of the average registration error within just seconds, there is still room for improvement. For example, the ICRP algorithm decreased the average registration error of the HSC algorithm from 0.037mm to 0.020mm for the registration of the block1-1-2 images. Thus, in the rest of the paper, we will always use the ICRP algorithm to refine the results obtained from registering the hierarchical segmented and clustered planar patches.

D. Comparative study

In this section, a comparative study is carried out based on real range images. All the algorithms show similar behaviour. Due to space limit, only 5 pairs of representative images (Figure 1) were used for the experiments: valve10-0, bunny80-60, cow42-39, bird20-60 and bunny100-60. These images were subject to camera motions with rotation angles as large as 40° around unknown axes and include free form surfaces with varied geometries and cluttered background. The experimental results are presented in Figure 5 and Table IV.

From Figure 5 and Table IV, it can be seen that all the three algorithms accurately registered both the valve10-0 and bunny100-60 images with the estimated rotation angles of the camera motions close to the expected ones. Even though the NSS method also successfully registered the bird20-60 images, it failed to register either the buddha20-0 or the cownum42-39 images. While the proposed HSC method also accurately registered the buddha20-0, cow42-39, and

TABLE I

THE AVERAGE e_μ AND STANDARD DEVIATION e_δ OF REGISTRATION ERRORS IN MILLIMETRES BASED ON RCS, EXPECTED AND CALIBRATED ROTATION ANGLES θ AND $\hat{\theta}$ IN DEGREES OF THE CAMERA MOTION, THE NUMBER N OF FINALLY ESTABLISHED RCS, AND REGISTRATION TIME t IN SECONDS FOR THE PROPOSED HSC ALGORITHM APPLIED TO DIFFERENT RANGE IMAGES WITH THE NUMBER α OF PATCHES REPRESENTED AS A PERCENTAGE OF THE NUMBER OF TOTAL POINTS IN THE ORIGINAL IMAGE TAKING DIFFERENT VALUES.

Image	α	e_μ (mm)	e_δ (mm)	θ $(^\circ)$	$\hat{\theta}$ $(^\circ)$	N	t $(sec.)$
lobster80-60	0.5	0.65	0.85	20	5.05	705	174
	1	0.41	0.33		18.69	4642	42
	10	0.41	0.33		18.69	4636	26
duck80-60	0.5	0.30	0.18	20	18.84	6614	32
	1	0.35	0.22		15.21	6391	35
	10	0.30	0.17		19.06	6570	33

TABLE II

THE AVERAGE e_μ AND STANDARD DEVIATION e_δ OF REGISTRATION ERRORS IN MILLIMETRES BASED ON RCS, EXPECTED AND CALIBRATED ROTATION ANGLES θ AND $\hat{\theta}$ IN DEGREES OF THE CAMERA MOTION, THE NUMBER N OF FINALLY ESTABLISHED RCS, AND REGISTRATION TIME t IN SECONDS FOR THE PROPOSED HSC ALGORITHM APPLIED TO DIFFERENT RANGE IMAGES WITH PLANAR PATCHES REPRESENTED USING DIFFERENT METHODS.

Image	PatchRep.	e_μ (mm)	e_δ (mm)	θ $(^\circ)$	$\hat{\theta}$ $(^\circ)$	N	t $(sec.)$
frog100-80	Centroid	0.31	0.14	20	19.48	7139	14
	ClosestPoint	0.31	0.14		19.52	7121	17
tubby100-80	Centroid	0.27	0.15	20	19.38	3129	6
	ClosestPoint	0.26	0.16		20.09	3101	6

TABLE III

THE AVERAGE e_μ AND STANDARD DEVIATION e_δ OF REGISTRATION ERRORS IN MILLIMETRES BASED ON RCS, EXPECTED AND CALIBRATED ROTATION ANGLES θ AND $\hat{\theta}$ IN DEGREES OF THE CAMERA MOTION, THE NUMBER N OF FINALLY ESTABLISHED RCS, AND REGISTRATION TIME t IN SECONDS FOR THE PROPOSED HSC ALGORITHM APPLIED TO DIFFERENT RANGE IMAGES WITH AND WITHOUT REFINEMENT.

Image	Refinement?	e_μ (mm)	e_δ (mm)	$\hat{\theta}$ $(^\circ)$	N	t $(sec.)$
block1-1-2	No	0.037	0.019	51.21	7108	3
	Yes	0.020	0.008	51.44	7591	78
Curvblock1-2	No	0.020	0.008	25.70	15087	8
	Yes	0.015	0.006	25.43	15585	10

TABLE IV

THE AVERAGE e_μ AND STANDARD DEVIATION e_δ OF REGISTRATION ERRORS IN MILLIMETRES BASED ON RCS, EXPECTED AND ESTIMATED ROTATION ANGLES θ AND $\hat{\theta}$ IN DEGREES OF THE CAMERA MOTION, THE NUMBER N OF FINALLY ESTABLISHED RCS, AND REGISTRATION TIME t IN SECONDS FOR DIFFERENT ALGORITHMS APPLIED TO DIFFERENT RANGE IMAGES.

Image	Algorithm	e_μ (mm)	e_δ (mm)	θ $(^\circ)$	$\hat{\theta}$ $(^\circ)$	N	t $(sec.)$
valve10-0	HSC	0.38	0.21	10	10.13	11058	19
	NSS	0.38	0.21		10.13	11060	6
	SI	0.38	0.21		10.12	11060	119
buddha20-0	HSC	0.58	0.24	20	20.20	10729	32
	NSS	0.92	0.62		2.62	8185	14
	SI	0.83	0.51		11.75	9282	176
cow42-39	HSC	0.71	0.39	30	29.91	2805	117
	NSS	0.87	0.53		154.38	507	283
	SI	1.05	0.81		43.14	996	240
bird20-60	HSC	0.30	0.16	40	40.31	2916	88
	NSS	0.31	0.18		40.39	2883	67
	SI	0.56	0.33		134.30	426	359
bunny100-60	HSC	0.24	0.13	40	40.08	2879	10
	NSS	0.24	0.13		40.11	2893	17
	SI	0.24	0.12		40.08	3583	35

Fig. 5. The registration results of different algorithms applied to different images. Top row: HSC; Middle row: NSS; Bottom row: SI. From left to right column: valve10-0, bunny80-60, cow42-39, bird20-60 and bunny100-60.

bird20-60 images, the SI method failed to register all of them. On average, the proposed HSC method reduced the average registration error of the NSS and SI algorithms by as much as 18.75% and 27.78% respectively, despite the fact that all their results were refined using the ICRP algorithm. This is because both the estimation of the normal vector in the NSS method and the spin image extraction in the SI method are sensitive to imaging noise, occlusion, appearance and disappearance of points in either image and both the normal space sampling in the NSS method and the uniform sampling in the SI method are not always effective to characterise the range images being registered. In contrast, the proposed HSC algorithm is essentially a deterministic two-phase scheme. The first phase is resistant to inaccurate segmentation and clustering. For example, a limited number of planar patches can hardly approximate the free form valve, buddha, cow, bird, and bunny surfaces. In this case, an advanced ICP variant is employed to register the closest points in the original images to their centroids, yielding reasonable registration results for the ICRP algorithm in the second phase to refine.

The NSS method is the most computationally efficient. This is because it usually converges pre-maturely, yielding poor results. The SI method is the most computationally expensive, since it has to match a sampled point of interest in one image to any sampled point in another. The proposed HSC algorithm makes a good tradeoff between registration accuracy and computational efficiency and thus, performs best on the whole.

IV. Conclusions

This paper proposes a novel algorithm for accurate and efficient range image registration. The novelty lies in that the intensively investigated hierarchical principal component analysis and k-means clustering approaches in the pattern recognition, data mining, and machine learning literature have been synthetically integrated into the process of range image registration for more efficient and accurate results. To the best of our knowledge, this is the first time ever that the hierarchical principal component analysis and k-means clustering approaches have been directly employed for such a purpose. Experimental results based on real range images captured using two different range scanners show that such integration is successful. Thus, it may open a novel avenue for accurate and efficient range image registration. Compared with the existing ones [5], [12], our algorithm has the following two advantages: (1) it operates on the given points themselves in the images without any feature extraction and matching and thus is easier to implement; and (2) it does not require a good initialization of registration parameters and has a much larger range for convergence and thus is more stable. The latter is in sharp contrast with the efficient ICP variants [12]. Despite the fact that they have an advantage of fast convergence, they require very good initialization of registration parameters, which is usually not available, as is the case for the experiments reported in this paper. Otherwise, they might fail. Further research includes investigating how the registration results in the first phase can be further improved and the computational time in the second phase can be further reduced.

Acknowledgements

B. Wei was supported by National Natural Science Foundation of China under grant No. 60673088.

References

[1] C.S.R. Aguiar, et al. Hierarchical segmentation for unstructured and unfiltered range images. *Proc. CGIV*, 2007, pp. 261-267.

[2] G. Dewaele, F. Devernay, and H. Horaud. Hand motion from 3D point trajectories and a smooth surface model. *Proc. ECCV*, 2004, pp. 495-507.

[3] S. Gold, A. Rangarajan, et al. New algorithms for 2-D and 3-D point matching: pose estimation and correspondence. *Pattern Recognition* 31(1998) 1019-1031.

[4] D. Huber, M. Hebert. Fully automatic registration of multiple 3D data sets. *IVC* 21(2003) 637-650.

[5] A. Johnson and M. Hebert. Using spin images for efficient object recognition in cluttered 3D scenes. *IEEE Trans. PAMI* 21(1999) 433-449.

[6] T. Jost, H. Hugli. A multi-resolution scheme ICP algorithm for fast shape registration. Proc. 3DPVT, 2002, pp. 540-543.

[7] Y. Liu, et al. Free form shape matching using deterministic annealing and SoftAssign. *Proc. ICPR*, 2004, pp. 128-131.

[8] Y. Liu. Replicator dynamics in the iterative process for accurate range image matching. *IJCV* 83(2009) 30-56.

[9] Y. Liu. Constraints for closest point finding. *PRL* 29(2008) 841-851.

[10] E. Lomonosov, et al. Pre-registration of arbitrarily oriented 3D surfaces using a genetic algorithm. *PRL* 27(2006) 1201-1208.

[11] T. Pajdla, L.V. Gool. Matching of 3-D curves using semi-differential invariants. *Proc. Int. Conf. ICCV*, 1995, pp. 390-395.

[12] S. Rusinkiewicz, M. Levoy. Efficient variants of the ICP algorithm. *Proc. 3DIM*, 2001, pp. 145-152.

[13] J. Santamaria, et al. A scatter search-based technique for pair-wise 3D range image registration in forensic anthropology. *Soft Computing* 11(2007) 819-828.